UNITED NATIONS EDUCATIONAL, SCIENTIFIC AND CULTURAL ORGANIZATION
INTERNATIONAL ATOMIC ENERGY AGENCY
INTERNATIONAL CENTRE FOR THEORETICAL PHYSICS
I.C.T.P., P.O. BOX 586, 34100 TRIESTE, ITALY, CABLE: CENTRATOM TRIESTE

H4.SMR/942-9

Third Workshop on 3D Modelling of Seismic Waves Generation Propagation and their Inversion

4 - 15 November 1996

Rayleigh Wave Group Velocity Tomography of Siberia, China and the Vicinity

[1] F. Wu, [2]A. Levshin, [3]V. Kozhevnikov

[1] Dept. of Geological Sciences
State University of New York
Binghamton, New York, U.S.A.

[2] Joint Seismic Program Center
Dept. of Physics
University of Colorado
Boulder, CO, U.S.A.

[3] Institute of Earth Crust
Russian Academy of Sciences
Irkutsk, Russia

Rayleigh Wave Group Velocity Tomography of Siberia, China and the Vicinity

Francis T. Wu

Department of Geological Sciences
State University of New York
Binghamton, New York 13902-6000

Anatoli L. Levshin

Joint Seismic Program Center
Department of Physics
University of Colorado
Boulder, Colorado 80309-0583

Vladmir M. Kozhevnikov

Institute of Earth Crust
Russian Academy of Sciences
Irkutsk, Russia

Abstract

Rayleigh waves are used in tomographic inversion to obtain group velocity maps of East Asia ($40°E-160°E$ and $20°N-70°N$). The period range studied is 30 to 70 seconds. Seismograms used for this study were recorded at CDSN stations, at a temporary broadband seismic array in Tibet, at several SRO stations, and Kirnos-equipped stations established in Asia by the former Soviet Union, in Siberia, in the Sakhalin and in Mongolia. Altogether more than 1200 paths were available in the tomographic inversion. The study area includes the Angara craton, the geologically ancient core of Asia, and the subsequently accreted units, the Altaids (a Paleozoic collision complex), the Sino-Korean platform (a chain of Archaen terranes separated by belts of active structures), the south China platform (a collage of Precambrain, Paleozoic and Mesozoic metamorphic and igneous terranes), as well as the Tibetan plateau (an active tectonic feature created in late Cenozoic through collision of the Indian subcontinent and the Asian continent). Many of these main units are recognizable in the tomographic images as distinctive units; Tibet appears as a prominent low velocity (about -15% from the average) structure, with western and central Tibet often appearing as the areas with the lowest velocities, the Central Asian fold-belt, and the Angara craton are consistently high group velocity areas. Some lesser tectonic features are also recognizable. For example, Lake Baikal is seen as a high velocity feature at periods greater than 40 seconds. However, the high group velocity feature does not stop near the southern end of Lake Baikal; it extends south-southwestward across Mongolia. The North China Plain, a part of the platform where extensional tectonics dominates, is an area of high velocities as a result of relatively thin crust. The south China block, the least tectonically active region of China, is generally an area of high velocity. For periods longer than 40 seconds, a NNE trending high group velocity gradient clearly exists in

eastern China; the velocities are noticeably higher in the east. From the group velocity maps, average dispersion curves at twelve locations were determined and inverted to obtain velocity structures. Main results of group velocity inversion include: (1) a Tibetan crust of around 60 km thick, with low crustal and upper mantle shear velocities, at 3.3 km/s and 4.2 km/s, respectively; (2) With the Moho constrained at 40-43 km, the Angara craton and the Central Asian foldbelt have a V_S in excess of 4.6 km/s; (3) relatively low shear velocities are obtained for tectonically active areas. In many parts of the study area, where Precambrian basement is exposed, the processes in the crust and upper mantle due to recent tectonic activities have modified the crust and upper mantle velocity structures under the Precambrian terranes; they are no longer underlain by high velocity crust and mantle.

Introduction

The purpose of this study is to investigate the lateral variations of crust and upper mantle seismic velocity structures in Siberia, China and their vicinity. Rayleigh wave group velocity is chosen as a datum because it is relatively easy to obtain a dense distribution of paths using the events in and on the periphery of the study area and the seismic stations internal to the study area. By combining data from the recently established high quality Chinese Digital Seismic Network (CDSN) stations and the upgraded Seismic Research Observatory (SRO) stations, data from a temporary network in Tibet (Owens et al., 1993), and a collection of data recorded at stations established by the former Soviet Union in Russia and Mongolia, we are able to obtain dispersion curves along more than 1200 paths. Most of the events used are too small for source mechanism solutions and thus we are not able to determine phase velocities using the single station method. Because of the size of events used (some as small as M4.3) and the limited response of the Kirnos sensors used at the former Soviet Union stations, we confine the period range of our study to between 30 and 70 seconds. Dispersion data in this range are sensitive to the crustal velocities and thickness and the S-wave velocity in the uppermost part of mantle; but due to the sparsity of the data, constraints must be applied to obtain meaningful results.

In a previous paper by the senior authors on group velocity tomographic study (Wu and Levshin, 1994; hereafter called paper I), both Rayleigh and Love group velocity maps for China were obtained. Although the area studied in Paper I is contained in the present area, the inclusion of new Rayleigh data recorded in Tibet and recent data at the CDSN and SRO stations greatly enhanced the path density. As a result, the resolution of the velocity maps for some areas has improved, and some of the features are changed somewhat. In this paper we shall emphasize the new tomographic results in northern Asia, but we will describe the results for other areas for the sake of completeness. For more details on velocity maps of China and vicinity and on methodology, the reader should refer to Paper I. For this paper, in addition to the tomographic maps, inversion of average group dispersion curves sampled at twelve locations from the images was performed to obtain the S-wave velocity structures. These structures provide a sample of the variations in crust and upper mantle.

The study area varies greatly in terms of basement geology and tectonic history. Fig. 1 shows the main tectonic units as well as the general topography. The names and criteria for division of the tectonic units as found in literature are different; for simplicity we shall follow those of Sengor et al. (1993) and Zonenshain et al, 1990) for the major units in northern Eurasia and the major tectonic

division as devised by Ren et al. (1986) in China. It is commonly agreed that the Asian continent grew as a result of accretion of smaller continental fragments (Zonenshain et al. 1990; Coleman, 1989). The geologically ancient Angara craton can be viewed as the core, around which the Altaids, a wide belt of Paleozoic subduction-accretion complex (Sengor et al., 1993), developed. The Altaids is bordered on the south by a Paleozoic to Mesozoic collision suture that has since become an active orogenic zone sometime during the Cenozoic. This zone includes the following mountains: Tienshan in Kyrgyzstan and western China, to the north of Tarim basin, Beishan near the Mongolian border and Yinshan in northeastern China. The North China-Korean platform, composed of a series of Precambrian blocks, the Tarim, the Alan Shan, the Ordos and North China Plain (Fig. 1), are underlain by Precambrian basement; these blocks are separated by presently active structures, and the North China Plain itself is undergoing extensional tectonics (Nabelek et al., 1987). South of this platform is the Paleozoic-Mesozoic suture along the Kunlun and the Astin Tagh mountain chain (north of the Tibetan plateau), the Nanshan (north of the Qaidam basin) and Qinling of eastern China. This is the suture along which Tibet and the South China block are attached to the rest of the continent. Except Qinling, the other parts of the suture has been reactivated. The western Tienshan is a very active tectonic zone, with intense seismicity, but eastern Tienshan, a belt of basins and ranges, is much less so (Figs. 1 and 2). The south China block was evidently attached to the rest of Asia in Permian, and it is one of the least active areas in China, except at its eastern edge, especially near Taiwan. It is underlain by Proterozoic to Mesozoic basement. The southern Tibetan block was accreted to northern Tibet in early Mesozoic and the impingement of the Indian plate along the Himalayan front that started about fifty million years ago had led to the formation of Tibet and the ongoing continental tectonics of the whole East Asian area (Molnar and Tapponnier, 1978). As shown in Fig. 1, many tectonic units are associated with distinct topographical expressions; thus the Angara craton, the Central Asian foldbelt, the Tarim basin are all easily distinguished.

The seismicity shown in Fig. 2 are events with $m_B > 4.5$ reported in the Preliminary Determination of Epicenters (PDE) by United States Geological Survey between 1977 and 1992. By comparing the seismicity in the continental area and the topography as shown in Fig. 1, a close relationship between them can be seen. The descent from the Pamir-Tibet plateau eastward to the plains in eastern China and north-northeastward to the western Siberian plains and the Angara highland is rather gradual; the seismicity attenuates also gradually from the Tibet-India border toward the north and northeast (Fig. 2). But where the topography terminates rather abruptly, as it is north of the Pamir-Tienshan, the seismicity also terminates relatively sharply. A few conspicuous seismically quiet areas can be distinguished in among the intensely seismic belts; these include the Tarim basin, the Ordos, the Ala Shan, the South China block, etc. Except for the South China block, these are identified as relatively rigid blocks that remain nearly undeformed among intensely deformed regions; they are underlain by Precambrian basement as described above. The South China block lies in the stress shadow zone and is not seismic in general.

Since the study area includes Precambrian terranes of substantial lateral extent amid active tectonic zones, close to the Himalaya/Tibet collision zone, as well some of the oldest cratons in Siberia that are are a few thousand kilometers away from the collision suture and nearly aseismic, it is interesting to see how the tectonic activities modify the crustal and upper mantle structures under these areas.

Elsewhere in the world, it is common to find that old shields are underlain by a high velocity lid (Brune and Dorman, 1963; Knopoff, 1983; Calcagnile and Scarpa, 1985; Snieder, 1988). Those areas, however, have not been subjected to recent tectonic activities. When rejuvenated tectonic activities are taking place, the deeper part of the crust and upper mantle under these terranes may be sufficiently modified by mantle processes and not be recognizable as such.

For Eurasia as a whole and using natural earthquakes as sources, Patton (1980) and Feng and Teng (1983) obtained the velocity structures of various portions by determining the Rayleigh wave dispersion curves for various parts of the area; while Patton (1980) defined the sub-regions based on topography and known crustal thickness, Feng and Teng (1983) divided the region into $10^{\circ} x 10^{\circ}$ grids; the paths used are relatively sparse in these studies because of the scarcity of data at the time and the resolution is rather coarse because of the grid size. For Siberia, a number of deep seismic profiles were made using artificial sources, and thus the crustal and mantle structures in that area are well delineated along those profiles. Egorkin et al. (1987) and Mechie et al. (1993) summarized the results along a number of profiles in the area of interest. We shall refer to these works in our discussion. Kozhevnikov and Barmin (1989) analyzed about 200 records of analog Soviet stations and several SRO stations deployed in Asia to obtain average Rayleigh wave group velocity curves for several pre-determined tectonic regions of Eastern Asia. These curves were used by Kozhevnikov et al. (1992) to find average lithosphere shear velocity structure for Tibet, the mountain region of Southern Siberia and Mongolia, platforms of South-eastern China and some other regions. With respect to Tibet, because of its unique tectonic characteristics, a number of studies were conducted. Chun and Yoshii (1977) used events on the eastern side of the Tibetan plateau and stations south of the Himalayas; they employed "regionalization" to obtain average crustal structure of the plateau. Brandon and Romanowicz (1986) employ the "two-event" technique to determine dispersion curves in northern Tibet. Bourjot and Romanowicz (1992) recently presented tomographic images of the Tibetan Plateau and its vicinity; they used two stations internal to China and several SRO stations in Asia and also ANTO in Turkey, GRFO in Germany and SSB in France. For the eastern part of China, Weir (1983) determined group velocities along several paths using three SRO stations.

In this paper, we shall first present and discuss the Rayleigh group velocity images obtained through tomographic inversion. In order to learn about the velocity structures of some key areas, we invert a number of averaged dispersion curves obtained from these images. The images and shear velocity models are then discussed in terms of their tectonic significance. We are particularly interested in the variation of crustal and upper mantle structures as a function of the age of the basement rocks and the intensity of recent tectonic activity.

Data

The data used for this study is a rather heterogeneous set, including Rayleigh dispersion data derived from three main sources: seismograms from M>6 earthquakes in Eurasia recorded at the Kirnos stations in the former Soviet Union collected by one of us (VMK), seismograms recorded at the SRO, CDSN and GSN stations in this region (obtained from IRIS/DMC), and finally data from a temporary network of 11 stations established in Tibet from July 1991 to June 1992 (Owens et al., 1993). Fig. 1

shows the locations of these stations. The inclusion of data from stations established by the former Soviet Union in Mongolia and Siberia is important as data from these areas were still somewhat lacking when this research was initiated. Altogether 261 paths from these stations were available. With the wide dynamic range for the CDSN, the upgraded SRO seismic systems, and the portable broad band stations on the Tibetan plateau, the records stay on scale for M_S = 6.5 earthquakes, and, in some cases, surface waves from M_S = 4.3 teleseismic events are recorded with good signal-to-noise ratio. Because most of the events used are smaller than M_S < 6) and also the limited response of the Kirnos instruments, group velocities determination is limited in the 30-70 seconds range. For the CDSN/SRO dataset, 150 events, which occurred in 1987, 1989, 1990, 1991 and the first half of 1992, were employed; the time spans used are related to the availability of data when they were acquired. With the temporary Tibetan array, we had, for the first time, extensive data internal to Tibet. Data from 30 events recorded at the array from July 1991 to June 1992 were used. All the events chosen for this study are located in and on the periphery of the area of interest. All in all, about 1200 event-station paths were finally chosen for the period range of 30-60 seconds; for 70 seconds period, however, only about half as many paths were available (Table I). The group velocity dispersion curves were determined with an interactive multiple filter group velocity program on a workstation, allowing rapid group velocity determination and visual quality control. Dispersion data are discarded when the sonogram shows complex envelop structures around the group arrival. In such cases we note that the waveform is usually more complex and relatively small, most probably radiated near the minimum of the radiation pattern and multipathing effects become pronounced.

Tomographic Methodology

To invert surface wave group velocities we applied a technique developed by Ditmar and Yanovskaya (1987) and Yanovskaya and Ditmar (1990). This technique can be considered a generalization of the Backus-Gilbert inversion method (Backus and Gilbert, 1968, 1970) for 2D problems. Input data for inversion are group travel times t_j for several fixed values T_m, $m = 1,...M$, of period T along given paths $L_i, j = 1,...J$, and corresponding cross-correlation matrices of travel time errors $R_t|_{T=T_m}$. Results of inversion are maps of group velocity distribution $U(\theta,\phi)|_{T=T_m}$ and a map of space resolution $R(\theta,\phi)$ for a given set of paths. Here θ and ϕ are latitude and longitude, respectively. The inversion procedure will be repeated for each period of interest. Much of the relevant theory behind the tomographic methodology is presented in paper I.

The 1D inversion

To invert for a one-dimensional structure at the particular geographical point we applied the following technique:

1. Extract the one-dimensional group velocity curve from a set of tomographic maps for different periods.

The value of the group velocity for given period T was extracted from the corresponding group velocity map. Let us select a geographical point with coordinates $r_0=(\theta_0,\phi_0)$. To avoid sharp kinks in the resulting dispersion curve, we applied a smoothing procedure:

$$\bar{U}(T,r_0)=\frac{\int U(T,r)\ W(r-r_0)\,dr}{\int W(r-r_0)\,dr}$$

where $r = (\theta,\phi)$. W is a Gaussian weight $W = e^{-\alpha(r-r_0)^2}$, and the value of α was taken to be 0.5.

2. Inversion of group velocity curve for the one-dimensional structure at given geographical point r_0.

We used with some modifications of an algorithm developed by Lokshtanov (Kushnir et al., 1989). This algorithm combines the conjugate gradient scheme with randomized choice of a starting model. The model is a flat-layered Earth with a fixed number of layers and free parameters. For inversion, a three layer model is usually used; except in the case of Tibet, where a four layered model is adopted. All shear velocities and all thicknesses of layers were considered as unknowns; in the initial model for each inversion, a significant jump in shear velocity between the second layer and the half-space is specified. Since the group velocity dispersion curve is sampled at only five periods, we have to use whatever constraints we have available in the inversion. By experimenting with various combinations of constraints (of Moho depth and velocities in the crust or mantle), we have decided to fix the Moho depth using results of deep seismic sounding near the sampling point when they are available, and determine the average S-velocities in the crust and in the upper mantle. In all the inversions, V_P were assumed to be 1.73 V_S, and densities were fixed.

We have also attempted a 3D inversion by applying the technique described above for 1D inversion to points of a regular grid covering region under study. We used a 2.6 degree increment in latitude and a 5.2 degree increment in longitude. The same parametrization of the model was used for each point. Bi-spline interpolation between points was used to obtain maps of different parameters such as the layer thickness or shear velocity at different depths.

Tomographic images and S-velocity inversion results

The path coverage we are able to obtain with our present dataset and the spatial resolution map for Rayleigh waves at 40 seconds are shown in Fig. 3a and b, respectively; they are representative of the path coverage and resolution for 30-60 seconds data. The total number of paths used for each tomographic inversion, the corresponding initial group velocities and the mean square residuals for resulting models are presented in Table I. At 70 seconds, the coverage is much less dense, mostly because of the limited energy for that period generated by the smaller events. Figs. 4a-e show the tomographic results for Rayleigh waves at 30, 40, 50, 60, and 70 second periods. To maximize the color scale contrast for these plots, we have chosen to set the minimum group velocity of each figure to red and the maximum to purple in the rainbow color scale. Note that the areas covered by the topographic map (Fig. 1) and the tomographic images and the resolution maps are the same.

It is important, when viewing the images, to know their resolution lengths. As shown in Fig. 3b, the length is on the order of 300-500 km in much of Tibet, where our path coverage is very dense; it deteriorates sharply near the edge of the study area, where the path coverage is poor (Figs. 3a and b). Features smaller than the resolution length for a particular area tend to be smeared. The images are sampled at twelve points, in the manner described above, to construct dispersion curves. The structures at the twelve points are chosen as representative of the large tectonic units within which the point lies.

The sampled dispersion curves are shown in Fig. 5. Of these twelve sites, we were able to find deep seismic sounding results at six of these points to constrain the Moho depths. The results of inversion are shown in Fig. 6. In this paper, all tomographic results were obtained assuming an isotropic model of the territory under study, previous experiment with anisotropy modeling did not yield significant result (see Paper I).

The velocity maps (Figs. 4a-e) show that, in general, the Rayleigh group velocities are high in the northern part of the area, in Siberia, and the Tibet plateau is the center of a low velocity closure. There are many details in these maps that can be discussed in terms of tectonics. To facilitate our description of the maps and the velocity models, we shall divide this area into seven sub-regions. More attention shall be given to well-resolved (with length <1000*km*) areas not discussed in paper I and areas where images are noticeably enhanced over those of Paper I; those areas well resolved in Paper I will be reviewed for the sake of completeness. As can be seen in Figs. 1 and 3b, the Urals are on the edge of better resolved area and the East European platform, in the northwestern corner of our maps, is not well resolved at all and thus we will not discuss it here. The general tectonics described below is based mainly on Zonenshain et al. (1990) and Sengor et al. (1993) for the northern part of the study area and on Ren et al. (1986) for the southern part.

1. Angara craton

The Angara craton (Fig. 1) is also called the Siberian platform (Zonenshain et al., 1990 and Egorkin et al., 1987). The craton is by no means uniform based on surface evidence. Rocks in the shield areas have isotopic ages as old as 3300-3650 Ma, and as a whole it probably became a continental landmass about 1700 Ma. Significantly, in various parts of the craton, there were extensive episodes of intraplate magmatism in Paleozoic and Mesozoic, flood basalt extrusion (255-245Ma) and kimberlite emplacement in Late Paleozoic and Mesozoic. Velocity models obtained along DSS profiles in this area (Yegorkin and Pavlenkova, 1981; Egorkin et al., 1987) show that it is underlain by crustal thickness varying from about 45 km in the central part of the craton to about 35 in the Vilyui depression in the southeast (Egorkin et al., 1987). This area is not known to be tectonically active in recent time; some of the epicenters shown in Fig. 2 may have been Peaceful Nuclear Explosion shots (Mechie et al., 1993).

The tomographic images reveal the craton to be an area of relatively high group velocity for the period range of 30-70 seconds. With the Moho depth constrained at 43 km (an average depth based on Egorkin et al., 1987), the inversion results ("65.110" in Figs. 6, and Table I) gives an average upper crustal V_S of 3.41, lower crustal V_S of 3.75 and an upper mantle V_S of 4.61 km/s.

2. Central Asian foldbelt

The foldbelt is situated to the west of the Angara craton and east of the Urals (Fig. 1) and it is bordered on the south by the Tienshan. It is noted that while the northern part of this area is a topographically flat area, the southern part rises gradually toward the south (Fig. 1). Sengor et al. (1993) deem it to be a part of the Altaids, formed in the Paleozoic as a result of progressive convergence between the Angara craton and North China (Zonenshain et al., 1990). It includes fragments of ancient massifs (1800 Ma-1900 Ma), oceanic complexes (1200-600 Ma), arcs, etc., and they were aggregated as a landmass in late Paleozoic. There is evidence for reactivation during late Paleozoic and early

Mesozoic. In terms of recent tectonics, the northern part is not presently active as shown by its lack of topographic expression and seismicity (Figs. 1 and 2), but the southern part, near the northwestern border of China and the border of Mongolia, the seismicity becomes noticeable.

Although this area is geologically younger than the Angara craton and has a different tectonic origin, together with the craton, these two areas form the high velocity core of Eurasia. In juxtaposition, the foldbelt has even a slightly higher velocity than that of the Angara craton, as can be seen especially in Figs. 4c and 4d. The sampled group velocity curve shown in Fig. 5 ("65.110"), together with that of the Central Asian foldbelt ("60.80"), are the highest in the study area. With the Moho constrained at 40 km (Egorkin et al., 1987), the average upper crustal velocity is 3.27 km/s, the lower crustal V_S is 3.86 and an upper mantle V_S of 4.63. These velocities are comparable to those under the Angara craton.

3. Lake Baikal and Mongolia

Lake Baikal and Mongolia belong to two different tectonic provinces based on geological history. While Lake Baikal lies within the Baykalides, a collision zone surrounding the Siberian platform that was formed somewhat earlier than the Altaids, Mongolia is within the Altaids (Fig. 1). It is well known that Lake Baikal is at the center of an active rift (Zorin et al., 1989), the crust under the rift was about 35 km, and the lithosphere is found to be very thin, on the order of 50 km, based mainly on gravity data.

While it is not surprising to see relatively high group velocity in the Lake Baikal area, as a result of thinned crust in a rift structure, the extension south-southwestward of the Lake Baikal group velocity high, at periods longer than 50 seconds, into central Mongolia was not expected. The flanking group velocity low in western Mongolia is more pronounced than that in the east. From Figs. 1 and 2, one can discern that western Mongolia is seismically more active and topographically more prominent than eastern Mongolia; this high group velocity ridge is essentially in the transition zone. In contrast to the Baikal area however, no corresponding topographic depression exists, although there are smaller north-south striking grabens in the northern part of the area (Baljinnyam et al., 1993). Three points along the group velocity high were sampled: the middle section of Lake Baikal ("53.108"), northern central Mongolia ("48.103") and southern Central Mongolia ("45.100"). All these locations are along the group velocity high. The sampled dispersion curves are shown in Fig. 5. The inversion for the Lake Baikal site, with the Moho depth constrained at 35 km (Yegorkin and Pavlenkova, 1981) yields a upper crustal V_S of 3.49 km/s, a lower crustal V_S of 3.75 km/s and an upper mantle V_S of 4.3 km/s Lake Baikal site ("53.108" in Figs. 5 and 6; Table 2). At the other two sites ("48.103" and "45.100") along the group velocity high, deep seismic profiling results are not available and the inversion was unconstrained; the crustal thicknesses obtained are greater than under Baikal, but because of the narrowness of the high group velocity area, the group velocity curves may not have been properly sampled.

4. Northeast Siberian Fold System

The northeast Siberian folds are bordered on the west by the Verhoyansk mountains, a mountain chain formed of Late Paleozoic through Jurassic shallow water clastic sediments, representing the passive margin of the Siberian continent. Its main interior consists of exotic blocks and a series of Jurassic to Cretaceous igneous bodies. It is close to the present day continental margin and the circum-Pacific subduction system. The Sikhote-Alin belt to the south of the Verhoyansk mountains is composed of

Cretaceous melange most probably associated with a subduction system.

The resolution of the tomographic images (Fig. 3b) deteriorates in eastern Siberia due to relatively sparse raypath coverage. At 70 seconds the northern part of the Verhoyansk mountains appear to be a relatively low velocity feature, but at all other periods, it is not distinguishable from the eastern edge of the Angara craton, but the Sikhote-Alin belt is a high velocity area. No velocity inversion was made for the Northeast Siberian fold belt because of the low resolution of our results. We inverted the Sikhote-Alin curve ("50.134" in Fig. 5) without constraining the Moho depth, and the result is shown in Fig. 6 and Table 2. It has a relatively thin crust of 35 km and low upper mantle velocity of 4.39 km/s.

5. Tibet and Southwestern China

The Tibetan plateau is composed of blocks that were successively accreted during the Mesozoic and early Tertiary. The formation of the plateau probably occurred after mid- to late-Miocene, and it is possible that major uplift occurred in Pliocene (Shackelton and Chang, 1988). Currently it is still a very active structure with frequent large earthquakes in its interior, especially toward the south, and the background seismicity is also fairly high (Fig. 2).

The low group velocity feature associated with the Tibetan plateau and its surrounding area dominate all tomographic images (Figs. 4a-e). At 30 seconds the Rayleigh image (Fig. 5a) exhibits an extensive low velocity feature that covers the northern Tibetan plateau as well as a large portion of the western Tarim basin, the Pamirs, eastern Afghanistan northern Pakistan and western Yunnan, west of station KMI (Fig. 1). Comparisons of the topography and the group velocity images show that at 40 seconds and longer period, the enclosed group velocity low correlate well with the outline of the plateau. However, near the southern margin, where the topography is the highest, Rayleigh group velocity increases rapidly. In general, the group velocity gradient is steeper in the south than in the east and the north, mimicking the way the topography changes in these areas. The extension to the west is evidently related to the Pamirs, but the resolution deteriorates in the southwest corner of the images, such that the exact shapes of the contours cannot be evaluated. The areas of the lowest velocity contours in Figs. 4b-e become smaller at longer periods, with its middle section increasingly pinched, until the contour splits into two at 70 seconds. With the shear wave velocities in the crustal and upper mantle column probably fairly similar across the plateau, the shape of the group velocity minimum at 60 and 70 seconds reflect the crustal thickness in Tibet (Paper I). At periods of 40-70 seconds, the Tarim and Qaidam basins are in the group velocity gradient zone.

Our tomographic images are quite comparable to those of Bourjot and Romanowicz's (1992). However, in their work the low velocity features are seen to persist up to 60 seconds, but as shown in Figs. 4a-e, we see it at 30-70 seconds, albeit the area is smaller at 70 seconds than at shorter periods. But with more paths available for our study, more details within the plateau start to appear.

The sampled group velocity curve for Tibet ("33.87" in Fig. 5) is very different from the other curves. The group velocity curve is essentially flat between 30 and 40 seconds. In comparison to the "pure path" dispersion curves of Feng and Teng (1983; region #45), the values are comparable at 30 seconds, but our values are lower at longer periods. The group velocities of Chun and McEvilly (1986) are significantly lower than our values at 30 and 40 seconds, and rise to velocities comparable to ours at

70 seconds. The unconstrained inversion results ("33.87" in Fig. 6) give a Moho depth of 60 km and a very low upper mantle S velocity of 4.23 km/s. The S velocities within the crust of 3.38 km/s are also low.

6. Tarim Basin and Tienshan

The Tarim basin is located in the southern part of the Altaids (Fig. 1); it is topographically quite distinct, as a relatively flat desert in among high mountains. Although the oldest rocks exposed in the basin (in western central Tarim along a thrust fault) are sedimentary rocks of Carboniferous age, the Basin is assumed to be underlain by Archaen basement, judged from outcrops on the rim of the basin (Ren et al., 1986). Remaining relatively undeformed while neighboring Tibet and western Tienshan were subjected to enormous N-S strain, the Tarim has been interpreted to be a rigid block. The area is seismically less active than the surrounding areas as shown in Fig. 2, but an E-W striking fault is seen through the desert sand (Remote Sensing Lab, 1978). Gravitationally it appears as a well-defined area of relatively high Bouguer anomalies (Paper I). It is therefore somewhat surprising that Tarim, with its east-west dimension on the order of 1000 km and north-south width in excess of 500 km, does not have a corresponding expression in the tomographic images, especially in view of the fact that the spatial resolution there is on the order of 500 km. In fact as we pointed out above, southwest and western Tarim is a region of relatively low group velocity and forms a part of the Tibet low group velocity anomaly for Rayleigh waves at 30, 40, 50 and 60 seconds (Figs. 4). Similar results were obtained by Bourjot and Romanowicz (1992). Tienshan was apparently a part of a Late Paleozoic suture. The western section of it, straddling across the Russian and Chinese border, is very active.

Because the Tarim basin is in a region of group velocity gradient, we did not attempt to construct an average group velocity curve. A group velocity curve is constructed in the western Tienshan area ("41.70" in Fig. 5) and when the Moho is constrained at 50 km, we obtain an average crustal velocity of 3.52 and an upper mantle velocity of 4.30 km/s.

7. Eastern China

The North China platform (includes areas marked #1 and #2, as well as North Korea, in Fig. 1) is composed of several blocks with different geological history and intensity of recent tectonics. The oldest rocks dated have isotopic ages of 3120 Ma (Yang et al., 1986). The North China Plain is underlain by a series of Neogene grabens developed in Proterozoic and perhaps older basement; the older rock are found on the edge of the basin. West of this Plain, the mountain front rises fairly steeply to a series of plateaus underlain by Archaen rocks. While the North China Plain is known to be active, mainly as an extensional basin under NNW tension (Nabelek et al., 1987), the older blocks west of the Plain, such as the Ordos platform, remain inactive (cf. Figs. 1 and 2). These blocks are, however, separated by active structures such as the Shenxi graben east of the Ordos platform.

The South China platform is separated from the North China platform by the Qinling mountains (Fig. 1); the northern edge of the Qinling is probably the suture along which the two parts of eastern China were hinged together in Permian (Yang et al., 1986). The basement of the South China platform is Proterozoic. In so far as young tectonics and seismicity are concerned, the South China platform as a whole is one of the least active parts of eastern Asia. Some seismicity is present in the southeast coastal China, near Taiwan, probably related to the collision tectonics there.

In the group velocity maps, especially in Figs. 4b-d, a high group velocity gradient in eastern China is seen to extend from just east of Mongolia to south China. This gradient is nearly coincident with the gradient in the topography (Fig. 1) and in Bouguer gravity (paper I); this zone is traditionally taken as the transition across which the Moho depth changes rapidly (Wang and Mao, 1985). Reflection and refraction profiles in this area (Wang and Mao, 1985) show that the crust is relatively thin with the Moho at about 32 km; it is a sharp decrease from the 40 km thick crust west of the transition. In our tomographic images, the North China Plain (Fig. 1) emerges as a region with relatively high group velocity at 40 seconds (Figs. 4b) and the region broadens westward at 50 and 60 seconds to include the Ordos platform (compare Figs. 1, 4b and 4c). The dispersion curve for the North China Plain area ("38.117" in Fig. 5), shows that the group velocity rises sharply until 60 seconds, and beyond that period the curve flattens. Thus, at 70 seconds (Fig. 4e) the North China plain is no longer a noticeable high velocity area. With the Moho depth constrained at 32 km (Wang and Mao, 1985), the resulting V_S in the upper crust is found to be 3.21 km/s, that of the lower crust 3.72 and that of the uppermost mantle 4.33 (Fig. 6, "38.117" and Table 2).

Much of the South China platform is a relatively high group velocity region at 40-60 seconds (Figs. 4b-d). A low velocity ridge, starting from southern Ryukyu and continue northwestward along a portion of the southern boundary of the North China-Korean platform, seems to exist at all periods studied (Figs 4a-e). This is an interesting feature that cannot easily be explained on the basis of surface geology or Bouguer gravity (Paper I). For south China the dispersion curve obtained in this study ("24.110" in Fig. 5) is fairly close to that of Weir (1982) and the constrained inversion with the Moho depth at 33 km yields an upper crust V_S of 3.32 km/s, that of the lower crust at 3.40 and that of the uppermost mantle at 4.27.

8. 3-D Inversion result

Fig. 7 shows the S-wave velocity distribution at 60 km, resulting from a 3-D inversion of the tomographic maps (Figs. 4a-e). Because the inversion is done on a fairly coarse grid (see Methodology), the velocity map obtained is highly smoothed. For most of the areas on this map, Fig. 7 shows the velocity in the upper mantle, but in Tibet, the S-wave velocity near the bottom of the crust is shown. At the other depth, the current results are too noisy for further study.

Discussion

The group velocity images at 30 to 70 seconds obtained from tomographic inversion of a densely distributed group dispersion dataset in eastern Eurasia provide us representations of the large scale crust and upper mantle structures. The resolution of the maps are not uniform, being better in China, where the modern digital stations began operation earlier than in other parts. However, the inclusion of analog data at stations in the former Soviet Union, equipped with Kimos seismometers, was important for resolving better the details in Siberia. In contrast to global tomographic studies (for example, Romanowicz, 1990; Montagner and Tanimoto, 1991), where the resolution length is on the order of 1000 km or more, the images presented in this paper, with spatial resolution of 300-500 km in much of the study area, have enough detail to compare to the regional scale tectonic features in Eurasia. Within Eurasia, the tectonic history varies greatly from region to region, and the Rayleigh group velocity

tomographic images shown in Figs. 4a-e allow us to associate surface tectonic features with deep structures. With the period ranging from 30 to 70 seconds, the maps indicate the variations of velocity structures in the lower crust and uppermost part of the mantle. Besides defining the structural units in terms of group velocity, the images also reveal some features that are not shown in surface geology. Furthermore, through constrained or unconstrained inversion of the group velocity dispersion curves derived from the tomographic images, the average S-wave velocity of the crust and upper mantle at key locations are obtained.

That the Angara craton is underlain by high velocity crust and uppermost mantle is consistent with observations in Precambrian terranes in Scandinavia and elsewhere (Snieder, 1988; Calcagnile et al., 1985). The Angara craton, together with the Central Asian foldbelt, a Paleozoic collision complex, form the high velocity core of Asia. The Central Asian foldbelt has thinner crust, and therefore appears as the area with the highest group velocity in the images (Figs. 4). We note that the Angara craton underwent significant extension in the Paleozoic and Mesozoic and has an higher average elevation (Fig. 1), resulting in a thicker crust. The younger Central Asian foldbelt has not had significant tectonic modification since its formation (Zonenshain et al., 1990). The absence of neotectonic activity in these areas indicates that the post-Tertiary reactivation of Eurasia as a result of impingement of the Indian subcontinent has not affected this area. The velocity structures determined from our dispersion curves for the Angara craton and the Central Asian foldbelt yield relatively high V_s in the crust and in the upper mantle.

There are many other geologically ancient terranes in this area as we have described earlier. They include the Ordos, Shanxi, the Alashan, the Sichuan basin, the North China Plain, etc. Unlike the Siberian shields, however, they do not show up as distinct high group velocity features. The size of these blocks are not as large as Siberia, but if the Lake Baikal rift as well as several other smaller units can be resolved as well as we have, then these features should be resolvable as well. While Ordos is noticeably aseismic (Fig. 2) and lacking other signs of recent tectonic activities, other terranes are either currently active, as are Shanxi, Alashan and the North China Plain, or in the vicinity of major active tectonic belts, such as the Tarim basin.

The Baikal rift south of the Angara craton is well known as an active feature (Zonenshain et al., 1990); the rift valley is a remarkable topographic feature and the area is seismically quite active (Fig. 2). The lithosphere in the rift valley area is found to be quite thin, about 40-50 km, and the crust is estimated to be less than 35 km, based on gravity and limited seismic data (Logatchev and Zorin, 1992). The high velocity ridge in the tomographic group velocity images as well as the high velocity swath in the 60 km S-wave velocity map (Figs. 4 and 7, respectively) are consistent with these results, although the group velocity inversion results give a much shallower Moho. Lacking constraints at the shorter period range could have biased our results toward lower velocities in the crust and therefore shallower Moho.

The continuation of the the Baikal rift high velocity feature into Mongolia was not suspected initially. Although little geophysical data are available in this area, Russian and Mongolian geologists have, on the basis of mainly gravity data, postulated that the area in Mongolia where the high velocity ridge is seen, is underlain by an upper mantle structure similar to that under the Baikal rift (see

Windley and Allen, 1993, for a review). Immediately south of Lake Baikal, there are several north-south striking rifts, the Hobsogol, Oka, etc., but further south, down to 46° S, there are only a few short and narrow grabens mapped. However, the area of high velocity nearly coincides with the area of late Cenozoic basaltic (Fig. 8; Windley and Allen, 1993). Our data is consistent with the existence of an "asthenosphere bulge" in this area. The Lake Baikal and the central Mongolian structures combine to form one of the major active tectonic element within the Eurasian continent.

The low velocity extreme in this area is exhibited by the Tibetan plateau. It represents the most prominent topography on the Earth and its subsurface structures have been under intense investigation (Him, 1988; Beghoul, Barazangi and Isacks, 1993; Zhao et al., 1994). The recent 1991-1992 broadband experiment on the plateau (Owens et al., 1993) increased the amount of surface wave data significantly. As a result, the spatial resolution of the group velocity images for the plateau area (Figs. 4a-e) is the shortest. The raypaths in the north-south direction however, are still relatively lacking. In that it is extremely difficult to deploy stations in the Tibetan interior, tomographic studies will probably provide the best chance to resolve the lateral variations of structures within the plateau. Our results already show that southern Tibet, near the Zangbo suture and the Himalayas, is a region of relatively high velocities, in comparison to the rest of the plateau. This result agrees with that of Jobert et al. (1985) obtained with instruments in southern Tibet. As far as the interior of the plateau is concerned, it appears that the plateau has a bowl shaped Moho with its bottom in central Tibet. Its extension westward toward the Pamirs is quite clearly expressed in the images. The unconstrained velocity inversion for the Tibetan plateau yields an average Moho depth of 60 km (Table 1). It has very low crustal velocity and low upper mantle velocity.

The extension of the Tibetan low velocity under southern Tarim, supposed to be a fairly rigid Precambrian block, is quite clearly shown in Figs. 4a-d. Tarim is not very active, seismically speaking, but the western part is known to have an E-W oriented active thrust fault (e.g., Ren et al., 1986). Thus, although it might be a region with geologically ancient basement, it is a currently active area. Judging from the fact that we can resolve more rapidly varying features such as the transition from central to southern Tibet, the gradual nature of this transition from Tibet to Tarim is real. It is also observed by Bourjot and Romanowicz (1992). It appears that tectonic activities under Tibet is spreading to the neighboring areas to the north.

We have noted earlier that the Tienshan fold belt as east of longitude $87°E$ (Fig. 1 and Paper I) is noticeably distinct from the western part in that whereas the western part reveals itself as an area with low Rayleigh wave group velocity, the eastern part is an area of relatively high velocity. This feature seems to be consistent with the observation that the Bouguer gravity low (Paper I) associated with western Tienshan (the -250 mgal contour) terminates there. Also, as noted earlier, the Tienshan here is actually a E-W striking basin and range province, with the presence of the sub-sea level Turfan basin as the lowest point. Evidently, this is a deep-seated feature, with a thin crust underneath, resulting perhaps from north-south tension. The seismicity of western section of Tienshan is rather high with large thrust events; in contrast, eastern Tienshan is not very seismic (Fig. 2).

The increase in group velocities of both the Rayleigh eastward across $105°E$ is clear in Figs. 4. The trend agrees generally with that shown in the Bouguer gravity map (Paper I). In the eastern half of

the study area, the relatively high velocity region south and east of Beijing (the North China Plain) is easily distinguished; it is evidently related to the thin crust in that region, with thickness generally less than 35 km (Wang and Mao, 1985). The North China Plain is a region of active extensional tectonics (Nabelek et. al., 1987) where many large earthquakes were located.

Southeastern China is also a region of relatively high velocities especially at periods less than 70 seconds. Here the thin Archaen crust (~32 km) is probably the main controlling factor. In contrast to the North China Plain, this region is not tectonically active. The Japan Sea area appears as a high velocity region for Love and Rayleigh waves at 40 seconds (Figs. 6a and 8a), but becomes an area of relatively low velocity for longer period Rayleigh waves (e.g., Fig. 6d and 6e).

Conclusion

The Rayleigh group velocity images of a large part of Eurasia reveal many features that can readily be correlated with known tectonics as well as interesting features not clearly seen from surface evidence. The geologically and topographically distinct Tibetan plateau is seen as a large well defined area with extremely low group velocities. The geologically ancient Angara craton is clearly shown as a high velocity entity. In terms of previously unsuspected features, the group velocity high extending southward from Lake Baikal to Mongolia is a good example. It is certain that we did not recover the full amplitude of the anomaly associated with Tibet, because we did not take into account the bending of rays. In fact, strong focusing and defocusing must occur, depending on the exact location of receivers, for rays passing through Tibet.

As a result of the establishment of new high quality digital stations in Eurasia, we can study the continental structures under Eurasia in more detail. In that Eurasia is very large and some parts are very remote, tomography provides a method for uniformly sampling the region and for resolving lateral variations. By using group velocity dispersion data as datum for this paper, we are able to obtain relatively high path density. With continued accumulation of data at the Global Seismic Network stations, one should be able to use data from larger earthquakes, for which the CMT solutions are available, and achieve similar path density.

Acknowledgement

This study was supported by National Science Foundation grants EAR-9004220 and EAR-9206545 and the Air Force Phillips Laboratory contract F1962890K0042 and NSF grant EAR9004220. We are thankful to Drs. Tatyana Yanovskaya and Paul Ditmar from the University of St.-Petersburg, Russia for providing us with their tomographic inversion program. We thank Dr. Dmitri Lokshtanov from Norsk Hydro, Norway for providing us with his program for group velocities 1D-inversion. We would like to thank Y. L. Kung, Robin Martin, R. J. Rau, and D. Salzberg of SUNY Binghamton for assistance. The IRIS/DMC in Seattle supplies all the Global Seismic Network data used in this study. Finally, we thank Alan Jones of SUNY Binghamton, who read the final draft and made editorial suggestions.

References

Backus, G. and Gilbert, F., 1968. The resolving power of gross Earth data. Geophys. J. Roy. Astro. Soc., 16: 169-205.

Backus, G. and Gilbert, F., 1970. Uniqueness in the inversion of inaccurate gross Earth data. Phil. Trans. Roy. Soc. London, 226: 123-192.

Baljinnyam, I., and 11 others, 1993. Ruptures of major earthquakes and active deformation in Mongolia and its surroundings. Geological Society of America Memoir 181, Boulder, Colorado, 62pp.

Beghoul, N., Barazangi, M., and Isacks, B.L., 1993. Lithospheric structure of Tibet and western North America: mechanism of uplift and comparative study, J. Geophys. Res., 98, 1997-2016.

Bourjot, L., and Romanowicz, B., 1992. Crust and upper mantle tomography in Tibet using surface waves. Geophys. Res. Lett., 19: 881-884.

Brandon, C., and Romanowicz, B., 1986. A "no-lid" zone in the central Chang-Thang platform of Tibet: Evidence from pure path phase velocity measurements of long period Rayleigh waves. J. Geophys. Res., 91: 6547-6564.

Brune, J.N., and Dorman, J., 1963. Seismic waves and Earth structure in the Canadian Shield. Bull. Seism. Soc. Am., 53: 167-509.

Calcagnile, G., and Scarpa, R., 1985. Deep structure of the European-Mediterranean area from seismological data. Tectonophysics, 118, 93-111.

Chun, K. Y., and McEvilly, T. V., 1986. Crustal structure in Tibet: High seismic velocity in the lower crust. J. Geophys. Res., 91, 10405-10411.

Chun, K. Y., and Yoshii, T., 1977. Crustal structure of the Tibetan Plateau: A surface wave study by a moving window analysis, Bull. Seismo. Soc. Am., 67, 737-750.

Coleman, R. G., 1989. Continental growth of Northwest China, Tectonics. 8, 621-635.

Ditmar, P.G., and Yanovskaya, T.B., 1987. A generalization of the Backus-Gilbert method for estimation of lateral variations of surface wave velocity. Izv. AN SSSR, Fizika Zemli (Solid Earth), no. 6: 30-60.

Egorkin, A.W., Zuganov, S.K., Pavlenkova, N.A., and Chernyshev, N.M., 1987. Results of lithospheric studies from long-range profiles in Siberia, Tectonophysics, 140, 29-47.

Feng, C. C., and Teng, T., 1983. Three-dimensional crust and upper mantle structure of the Eurasian continent. J. Geophys. Res., 88: 2261-2272.

Hirn, A., 1988. Features of the crust-mantle structure of Himalayas-Tibet: a comparison with seismic traverses of Alpine, Pyrenean and Variscan orogenic belts. Phil. Trans. Roy. Soc. London. A 327: 17-32.

Jobert, N., Jounet, B., Jobert, G., Hirn, A., and Sun, K.Z., 1985. Deep structure of southern Tibet inferred from the dispersion of Raleigh waves through a long-period seismic network, Nature, 313, 386-388.

Knopoff, L., 1983. The thickness of the lithosphere from dispersion of surface waves, Geophys. J. Roy. Astro. Soc., 74, 55-81.

Kozhevnikov, V.M. and Barmin, M.P., 1989. Dispersion curves of Rayleigh wave group velocities for several regions of the Asian continent. Izv. AN SSSR, Fizika Zemli (Solid Earth), no. 9: 16-25.

Kozhevnikov, V.M., Lokshtanov, D.E. and Barmin, M.P., 1992. Shear-velocity structure of the lithosphere for nine large tectonic regions of the Asian continent. Izv. AN SSSR, Fizika Zemli (Solid Earth), no. 1: 61-70.

Kushnir, A.F., Levshin, A.L., Lokshtanov, D.E., 1989. Determination of the velocity cross-section from the spectra of surface waves by nonlinear optimization methods. In: "Problems of Seismological Information Science, Comput. Seismology", ISS. 21, Allerton Press, NY, 127-141.

Logatchev, N.A., and Zorin, Yu.A., 1992. Baikal rift zone; structure and geodynamics, Tecontophysics, 208, 273-286.

Mechie., J., Egorkin, A.V., Fuchs, K., Ryberg, T., Solodilov, L., Wenzel, F., 1993. P-wave mantle velocity structure beneath northern Eurasia from long-range recordings along the profile Quartz, Phys. Earth and Planet. Inter.: 79, 269-286.

Molnar, P. and Tapponnier, P., 1978. Active tectonics of Tibet, J. Geophys. Res., 83: 5361-5375.

Montagner, J.P. and T. Tanimoto, 1991. Global upper mantle tomography of seismic velocities and anisotropy, J. Geophys. Res. 96, 20337-20351.

Nabelek, J., Chen, W.P., And Ye, H., 1987. The Tangshan earthquake sequence and its implications for the evolution of the North China Basin. J. Geophys. Res., 92: 12615-12628.

Owens, T.J., Randall, G.E., Wu, F.T. and R.S. Zeng, 1993. PASSCAL instrument performance during the Tibetan plateau passive seismic experiment, Bull. Seism. Soc. Am., 83, 1959-1970.

Patton, H., 1980. Crustal and upper mantle structure of the Eurasian continent from the phase velocity and Q of surface waves. J. Rev. Geophys. Space Phys. 18: 605-625.

Remote Sensing Lab., 1978. ERTS images of China, Geology Publisheres, Beijing, 537p.

Ren, J.S., Jiang C.F., Zhang, Z.K. and Qin, D.Y., 1986. Geotectonic Evolution of China. Springer-Verlag, New York, 203p.

Romanowicz, B., 1990. The upper mantle degree 2: Constraints and inferences on attenuation tomography from global mantle wave measurement, J. Geophys. Res. 95, 11051-11071.

Sengor, A.M.C., Natal'in, B.A., and Burtman, V.S., 1993. Evolution of the Altaid tectonic collage and Palaeozoic crustal growth in Eurasia. Nature: 364, 299-307.

Shackelton, R.M. and C.F. Chang, 1988. Cenozoic uplift and deformation of the Tibetan plateau: the geomorphic evidence. Phil. Trans. Roy. Soc. London. A 327: 365-377.

Snieder, R., 1988. Large-scale waveform inversions of surface waves for lateral heterogeneity, 2. Application to surface waves in Europe and the Mediterranean. J. Geophys. Res., 93, 12067-12080.

Terman, M., 1973. Tectonic Map of China and Mongolia. Geol. Soc. of Am., Boulder, Colorado.

Wang, G.Z., and Mao, E.T., (Eds.) 1985. Crust and Upper Mantle in China, Results of Geophysical Exploration. Seismological Press, Beijing, China.

Wier, S. 1982. Surface wave dispersion and Earth structure in South-Eastern China. Geophys. J. Roy. Astr. Soc., 69: 33-47.

Windley, B.F., Allen, M.B., 1993. Mongolian plateau: Evidence for a late Cenozoic mantle plume under central Asia, Geology, 21, 295-298.

Wu, F.T., and A. Levshin, 1994. Surface-wave group velocity tomography of East Asia, Phys. of Earth and Planet. Int., 84: 59-77.

Yang, Z.Y., Cheng, Y.Q., Wang, H.Z., 1986. The Geology of China. Clarenden Press, Oxford.

Yanovskaya, T.B. and Ditmar, P.G., 1990. Smoothness criteria in surface wave tomography. Geophys. J. Int., 102: 63-72.

Yegorkin, A.V. and Pavlenkova, N.I., 1981. Studies of mantle structures of U.S.S.R. territory on long-range seismic profiles, Phys. of Earth and Planet. Int., 25, 12-26.

Zhao, Wenjin, Nelson, K.D., and Project Team, 1994. Deep seismic reflection evidence for continental underthrusting beneath southern Tibet, Nature, 366, 557-559.

Zonenshain, L.P., Kuzmin, M.I., and Natapov., L.M., 1990. Geology of the USSR: A plate-tectonic synthesis, Geodynamics ser. vol. 21, Am. Geophys. Union, Washington, D.C.

Zorin, Yu.A., Kozhevnikov, V.M., Novoselova and Turutanov, E.K., 1989. Thickness of the lithosphere beneath the Baikal rift zone and adjacent regions, Tectonophysics, 168, 327-337.

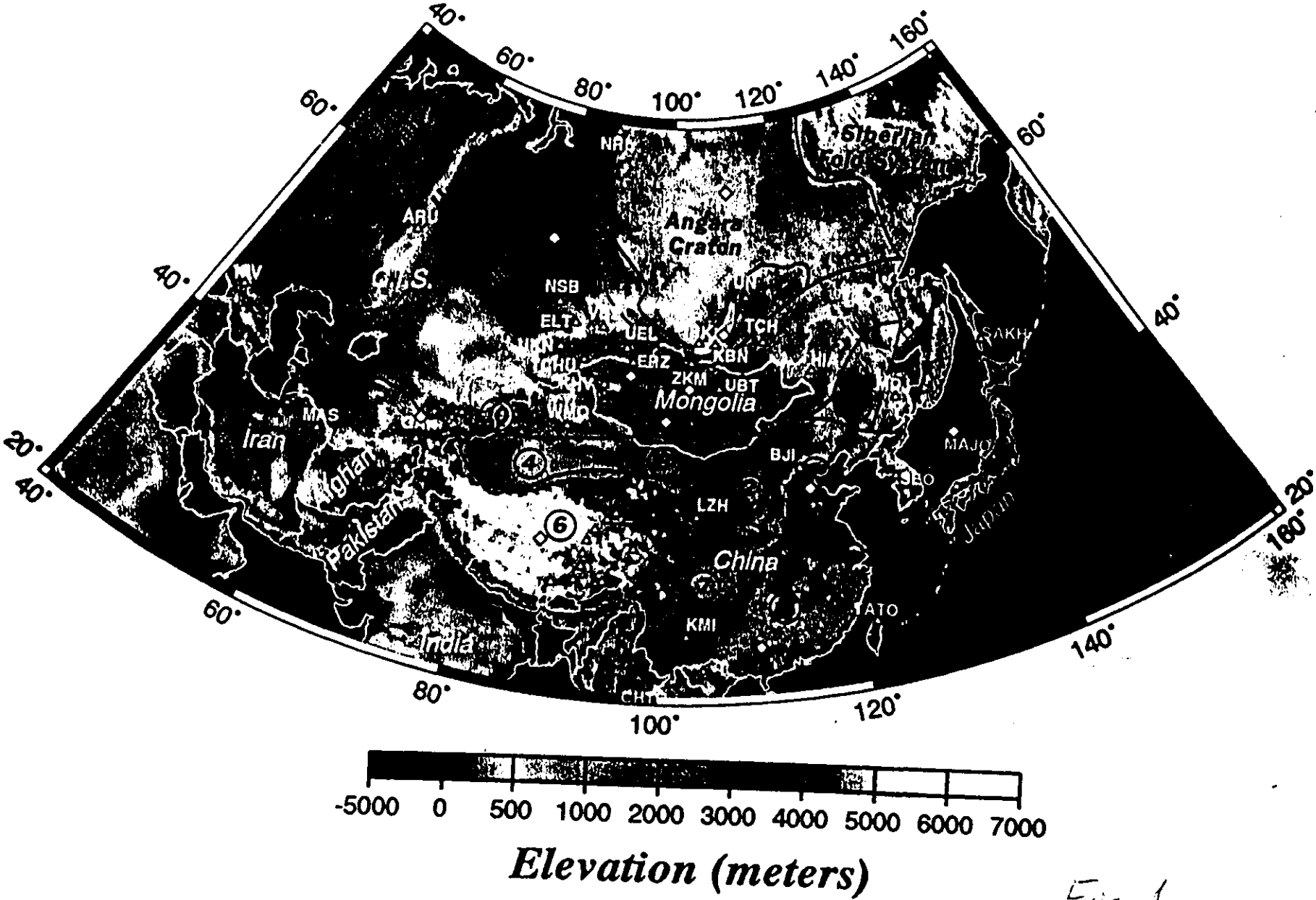
40°
60°
80°
100°
120°
140°
160°
20°
NRIL
ARU
C.I.S.
NSB
ELT
UEL
TCH
EAZ
XBN
ZKM
UBT
Angara Craton
Siberian Platform
Mongolia
Iran
Afghan.
Pakistan
India
China
Japan
BJI
LZH
MAJO
SEO
KMI
ATO
SAKH
CHT
-5000
0
500
1000
2000
3000
4000
5000
6000
7000
Elevation (meters)

Fig. 1

Figures

Figure 1. Topography of Eastern Asia based on the ETOPO5 topographic database with generalized tectonics superposed (after Sengor et al., 1993 and Terman, 1973). The numbered features are (1) North China Plain, (2) The Ordos Platform, (3) the Ala Shan Block, (4) The Tarim Basin, [these four, together with North Korea, are often collectively called North China-Korean Platform], (5) Qaidam Basin, (6) Tibetan Plateau, (7) Sichuan Basin, (8) South China Platform, (9) Sung-Liau Plain and (10) Tienshan. The locations of seismic stations used in the study are shown as triangles. Station CHTO is below latitude 20 at longitude 100 E. The HIA, MDJ, BJI, LZH, WMQ and KMI are part of the Chinese Digital Seismographic Network (CDSN). The stations in the former Soviet Union and Mongolia, except ARU, KIV, GAR and AAK, which are now a part of the Global Seismic Network, are stations established by the former Soviet Union. Notice that many of the tectonic units shown in this figure are clearly associated with major topographical features. The Tibetan Plateau is the most prominent feature on this map. Some of lesser features can be seen in this map. For example, although the eastern section of Tienshan southeast of WMQ station is a continuation of the western Tienshan, it is actually a basin and range area with its lowest point in the Turfan Basin (-280m). The Szechuan Basin (#7, the bluish area north of KMI station) is surrounded by 1000-2000 mountain ranges. The general decrease in topography from Tibet to western China can be clearly seen. The diamonds mark the location where average dispersion curves are constructed and one dimensional velocity structures obtained.

Figure 2. Seismicity of the study area. Data include epicenters of all events of M>4 from 1977-1992 published by USGS in the Preliminary Determination of Epicenters (PDE). The epicenters are marked as circles.

Figure 3. (a) Path coverage for this study. Along most of the paths both Love and Rayleigh waves are available. For different periods the coverage varies slightly. (b) Resolution of tomographic inversion results for Rayleigh Waves at 50 seconds.

Figure 4. Rayleigh wave group velocity tomographic inversion results for (a) 30 seconds, (b) 40 seconds, (c) 50 seconds, (d) 60 seconds, and (c) 70 seconds. Note that a different velocity scale is used for each figure.

Figure 5. Group velocity data (points) obtained by taking an average value around the points marked by diamond in Fig. 1 and the synthetic curves calculated from inversion models. The numbers in each frame correspond to the latitude and longitude of the sampling point.

Figure 6. Velocity structures obtained at twelve locations shown in Fig. 1. The numbers in each frame correspond to the latitude and longitude of the sampling point.

Figure 7. S-wave velocity at 60 km depth, obtained by inverting the group velocity maps.

Figure 8. The location of the high group velocity feature in central Mongolia (defined by the 3.6 and 3.7 km/s contours, and its relation to the occurrence of late Cenozoic basaltic volcanics (after Windley and Allen, 1993).

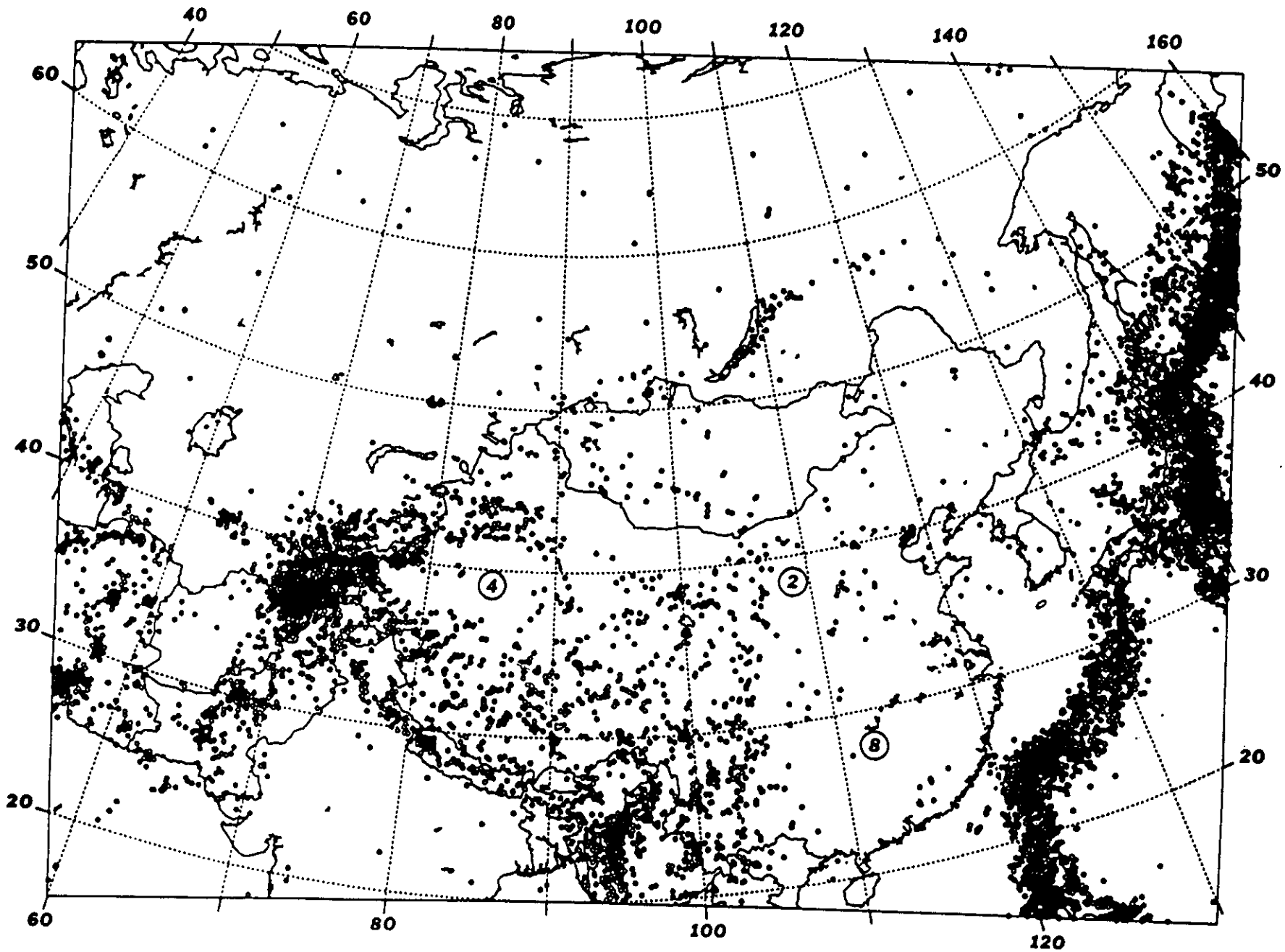

Fig. 2

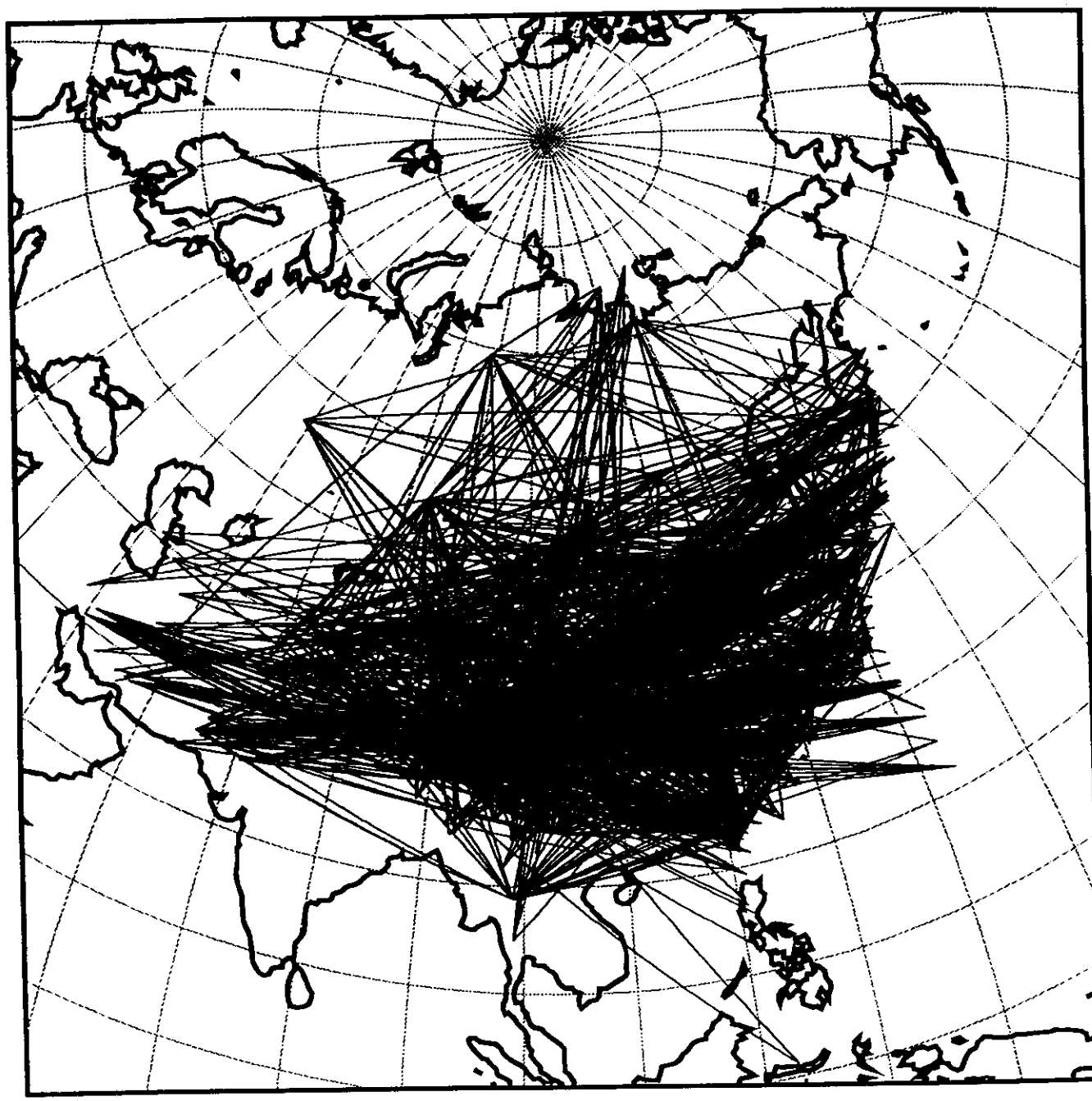

Fig. 3a

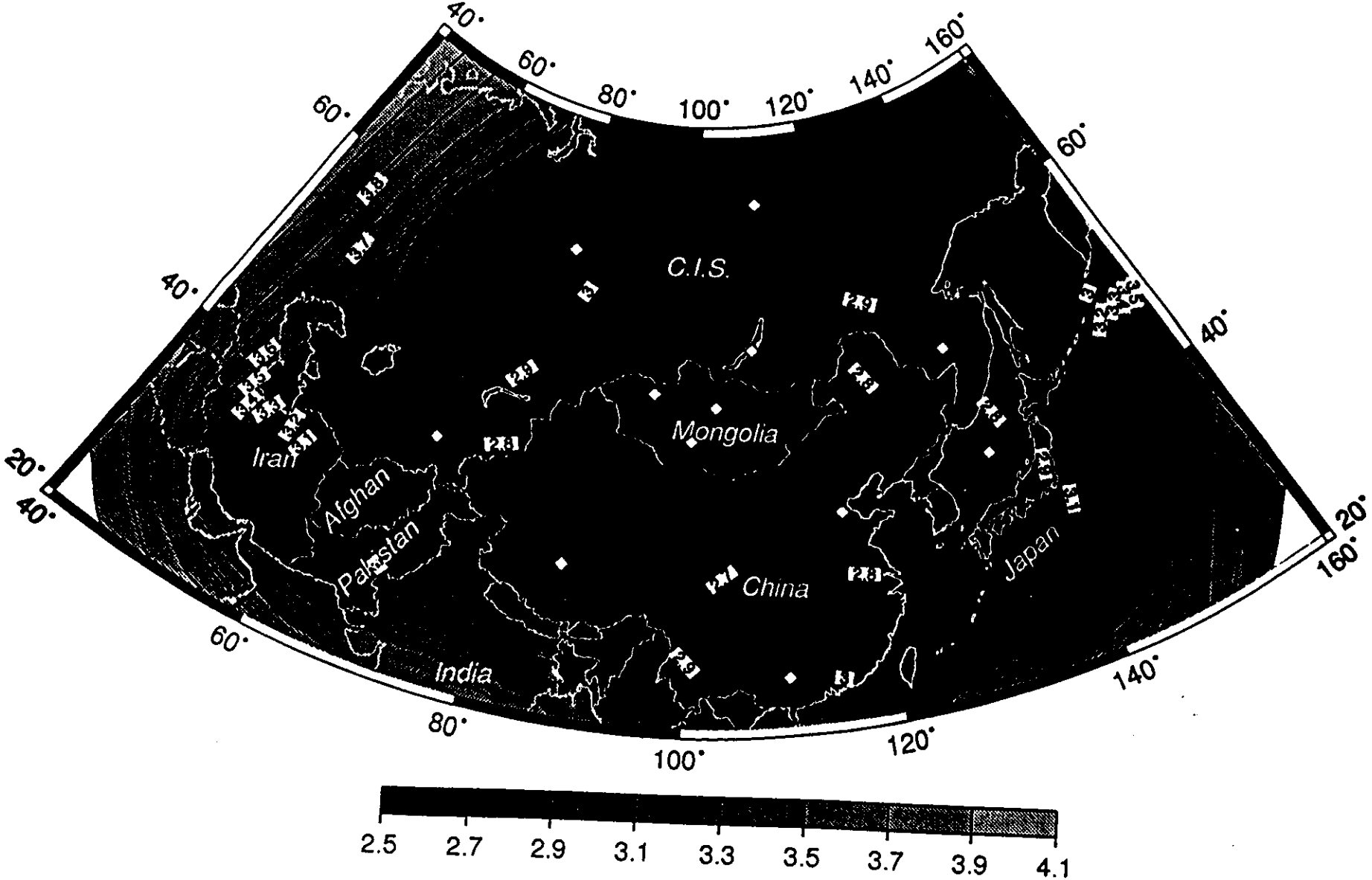
40°
60°
80°
100°
120°
140°
160°
20°
C.I.S.
Mongolia
Iran
Afghan
Pakistan
China
India
Japan
2.5
2.7
2.9
3.1
3.3
3.5
3.7
3.9
4.1

Fig 36

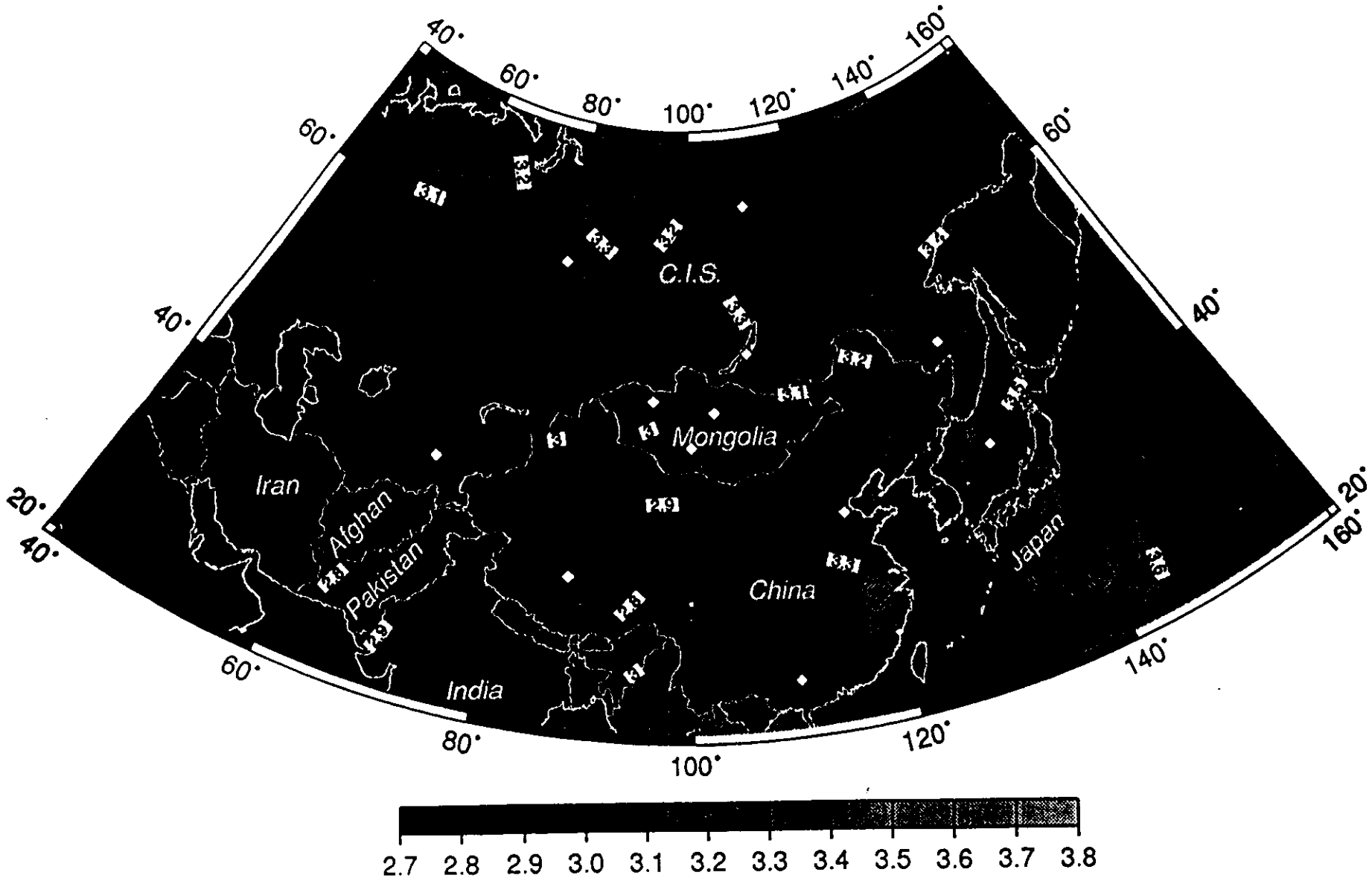
40°
60°
80°
100°
120°
140°
160°
20°
C.I.S.
Mongolia
Iran
Afghan
Pakistan
India
China
Japan
2.7
2.8
2.9
3.0
3.1
3.2
3.3
3.4
3.5
3.6
3.7
3.8

Fig 4a

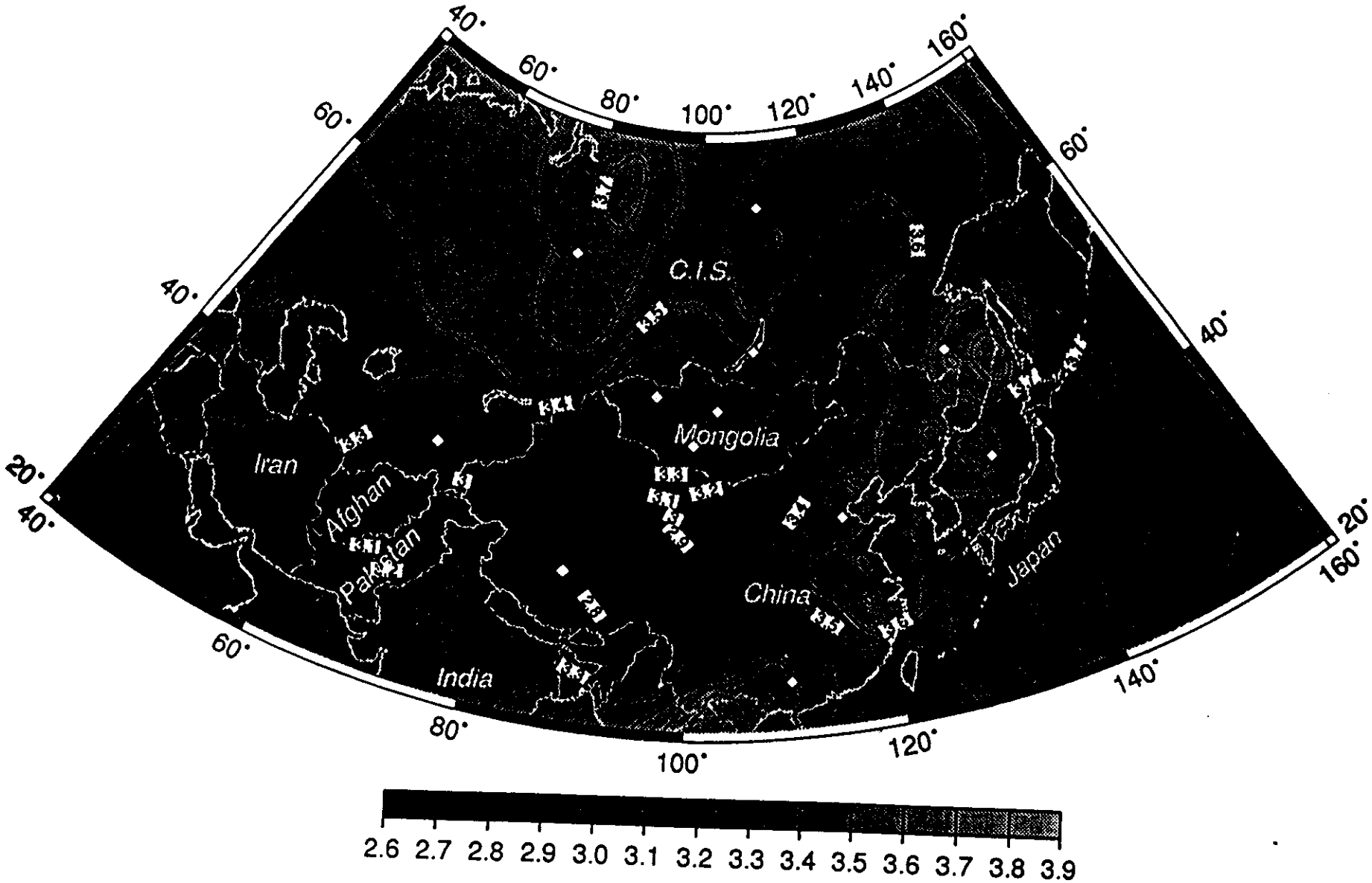
40°
60°
80°
100°
120°
140°
160°
20°
C.I.S.
Mongolia
Iran
Afghan
Pakistan
India
China
Japan
2.6 2.7 2.8 2.9 3.0 3.1 3.2 3.3 3.4 3.5 3.6 3.7 3.8 3.9

Fig 46

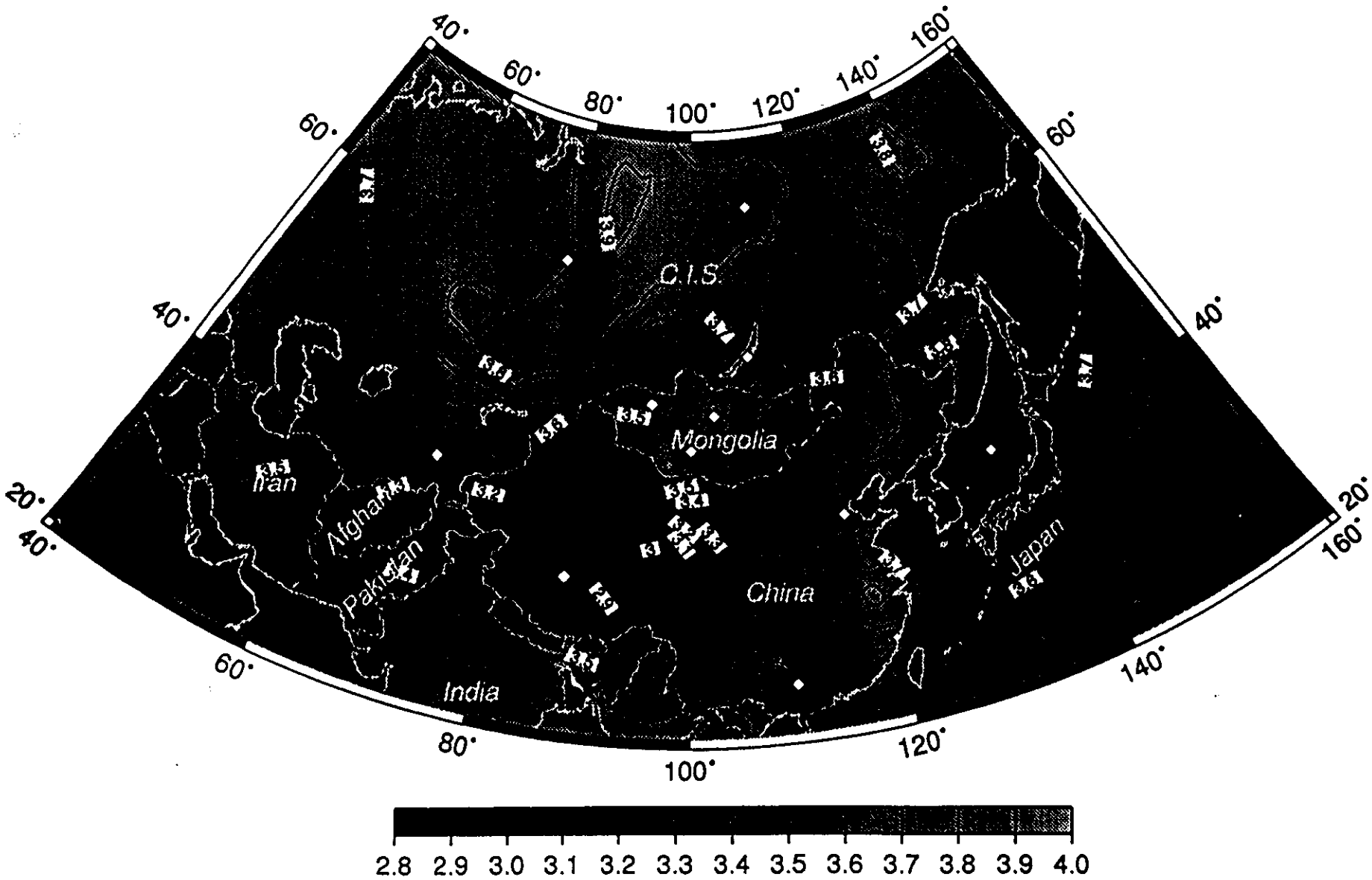
40°
60°
80°
100°
120°
140°
160°
20°
C.I.S.
Mongolia
Iran
Afghanistan
Pakistan
India
China
Japan
2.8 2.9 3.0 3.1 3.2 3.3 3.4 3.5 3.6 3.7 3.8 3.9 4.0

Fig 4c

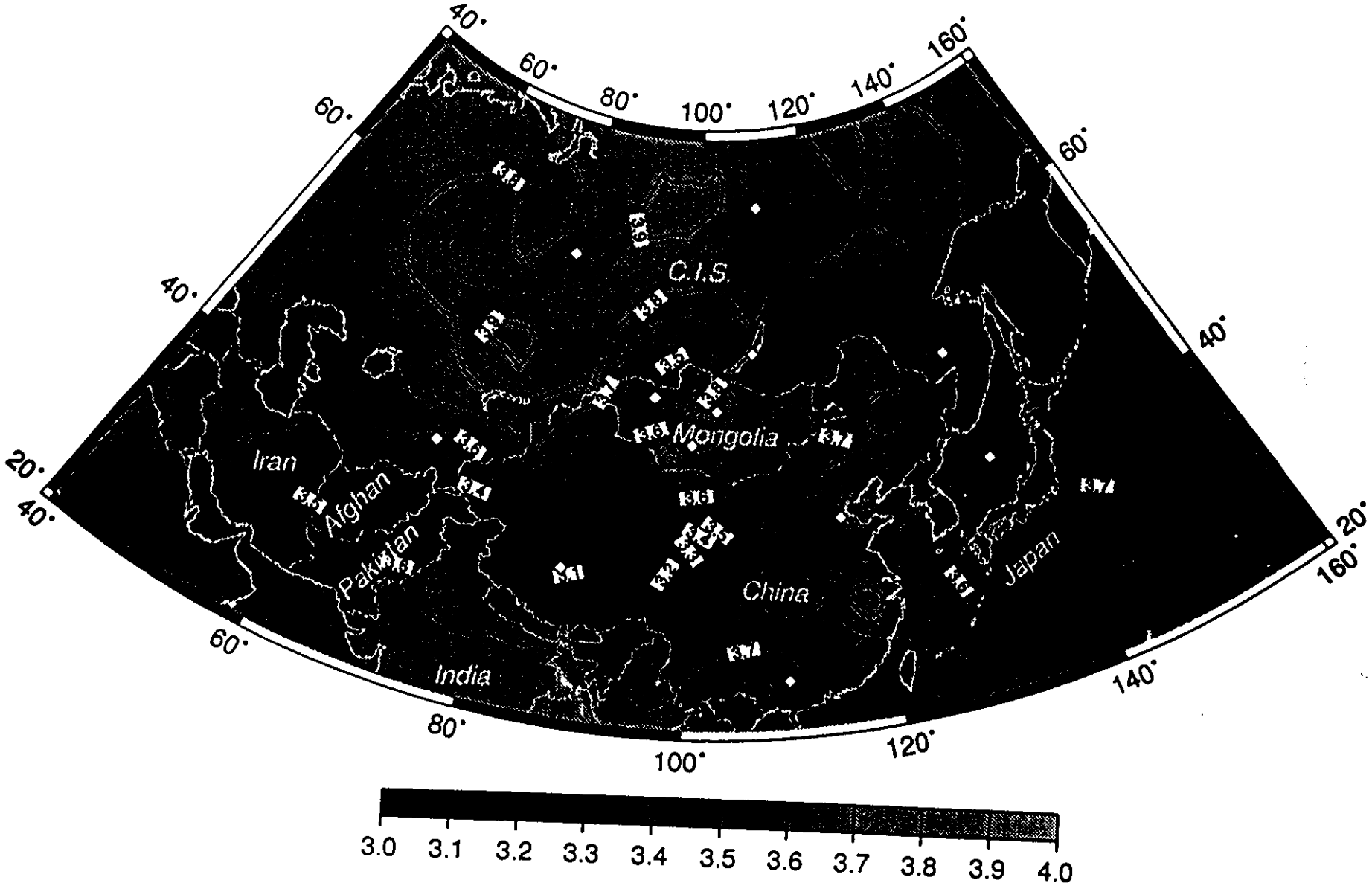
40°
60°
80°
100°
120°
140°
160°
60°
40°
20°
C.I.S.
Mongolia
Iran
Afghan
Pakistan
China
India
Japan
3.0
3.1
3.2
3.3
3.4
3.5
3.6
3.7
3.8
3.9
4.0

Fig 4d

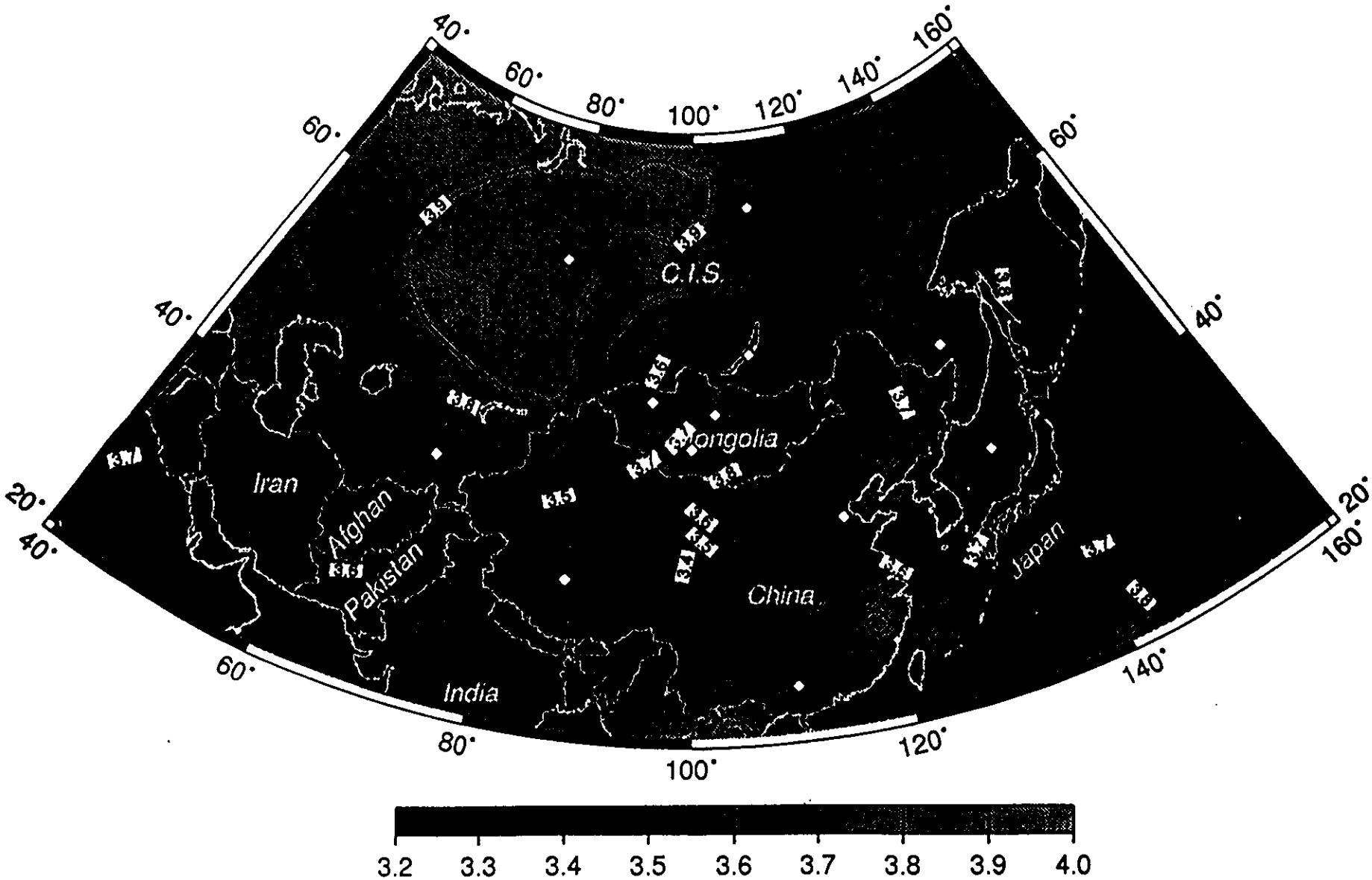
40°
60°
80°
100°
120°
140°
160°
20°
C.I.S.
Mongolia
Iran
Afghan
Pakistan
India
China
Japan
3.2
3.3
3.4
3.5
3.6
3.7
3.8
3.9
4.0

Fig 4e

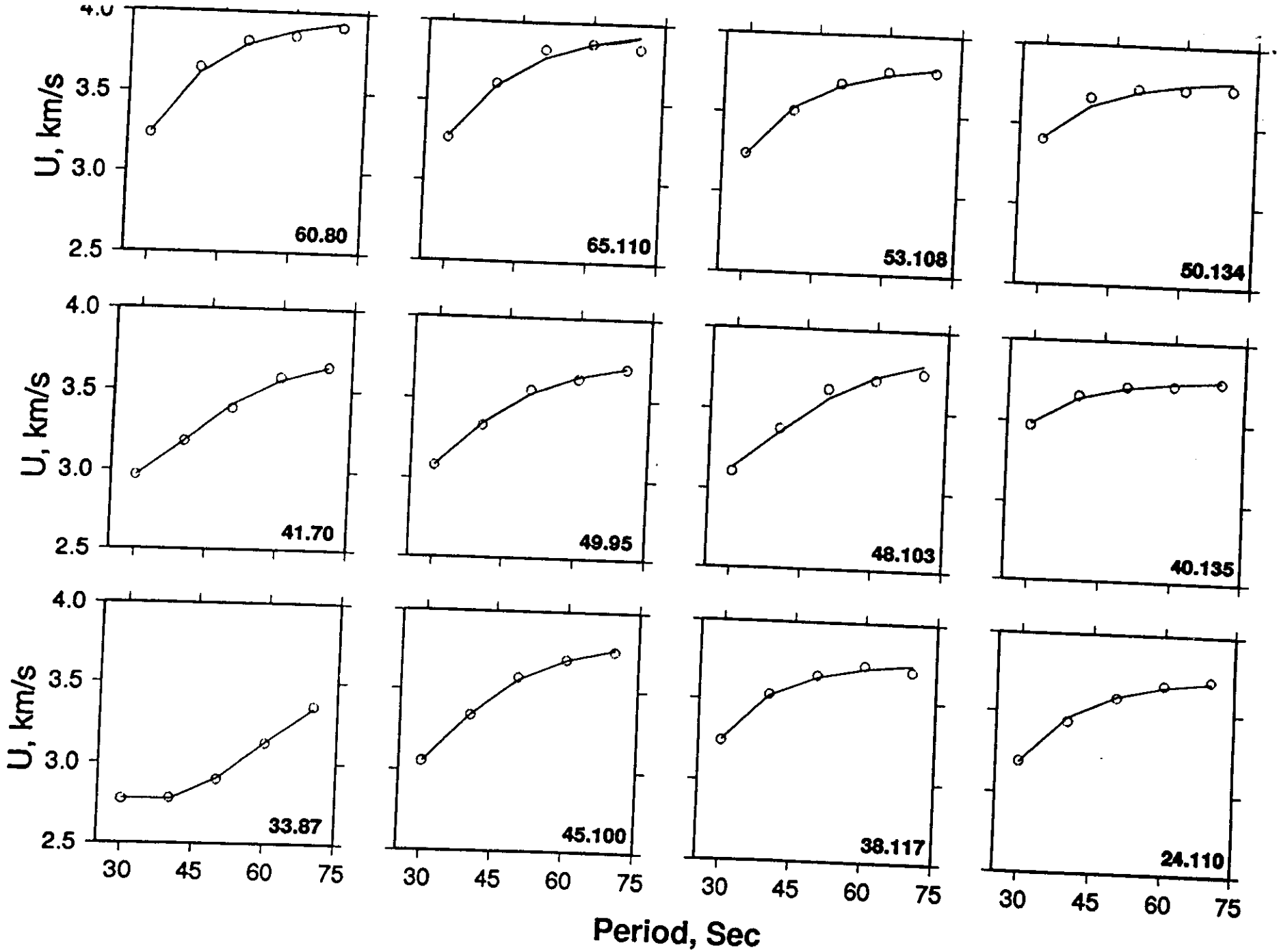
U, km/s
4.0
3.5
3.0
2.5
60.80
65.110
53.108
50.134
41.70
49.95
48.103
40.135
33.87
45.100
38.117
24.110
30
45
60
75
Period, Sec

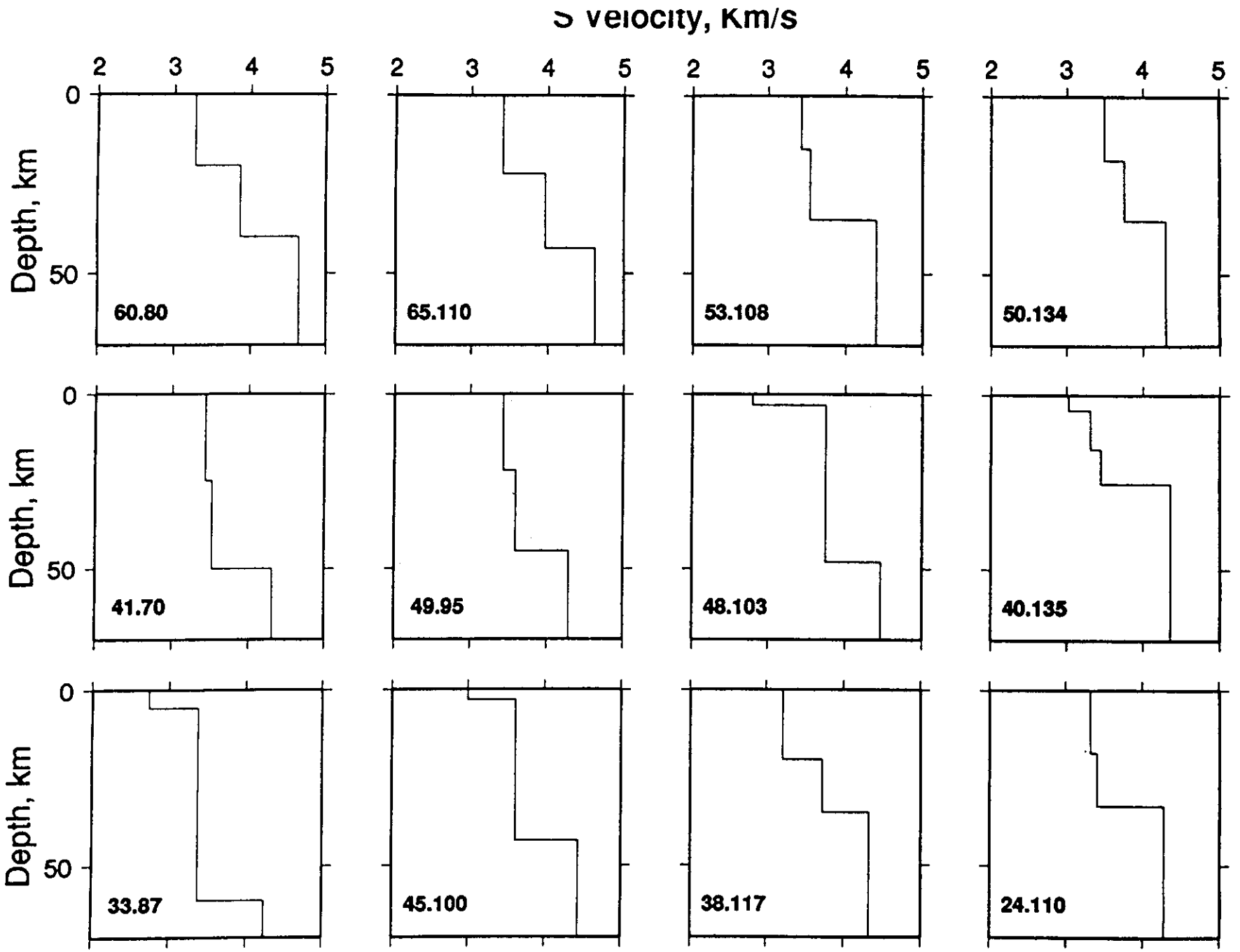
S velocity, Km/s
2
3
4
5
0
50
Depth, km
60.80
65.110
53.108
50.134
41.70
49.95
48.103
40.135
33.87
45.100
38.117
24.110

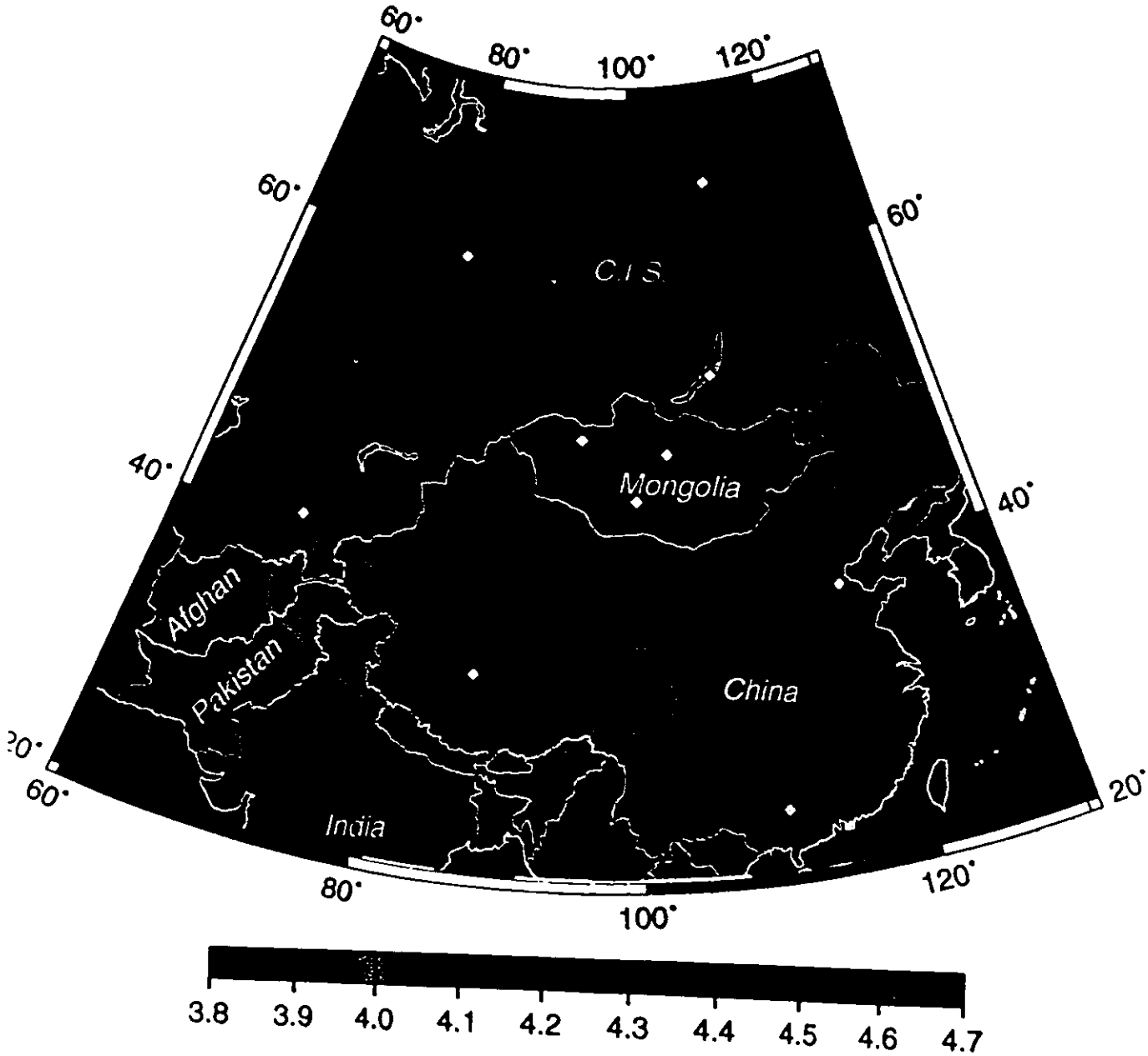
60°
80°
100°
120°
60°
60°
60°
C.I.S.
40°
40°
Mongolia
Afghan
Pakistan
China
20°
60°
India
80°
100°
120°
20°
3.8
3.9
4.0
4.1
4.2
4.3
4.4
4.5
4.6
4.7

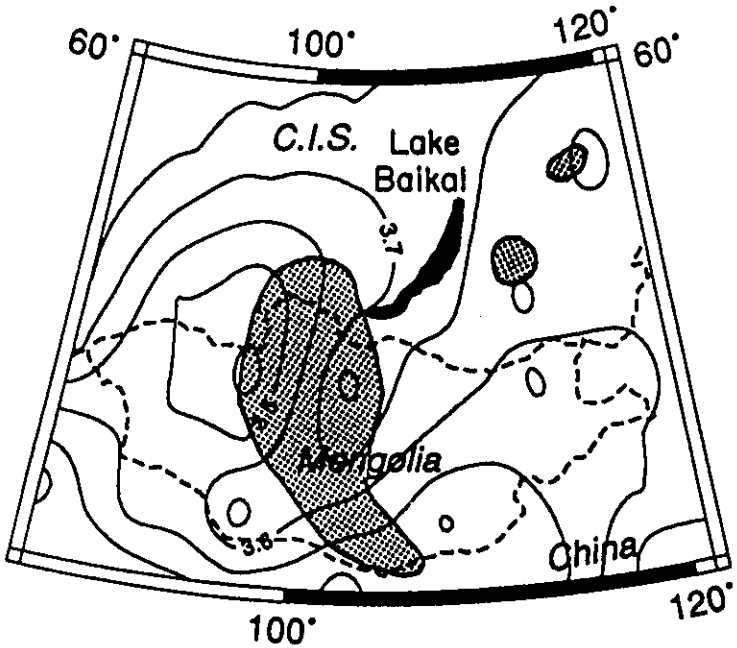
60°
100°
120°
60°
C.I.S.
Lake
Baikal
3.7
Mongolia
3.6
China
100°
120°

Table 1

Inversion parameter and residuals for different waves and periods

Period Sec	Number of paths	Average velocity km/s	Average residual Sec
30	1165	3.09	31.8
40	1158	3.30	32.0
50	1109	3.45	29.5
60	935	3.58	24.7
70	511	3.63	21.8

Table 2 Velocity Models, * denotes constrained inversion result with Moho depth fixed.

W. Siberian		Angara		Baikal		E. Russia*	
depth	velocity	depth	velocity	depth	velocity	depth	velocity
0.	3.27	0.	3.41	0.	3.49	0.	3.42
20.	3.86	22.	3.96	18.	3.75	15.	3.53
40.	4.63	43.	4.61	35.	4.30	35.	4.39

Pamir		W. Mongol.*		C. Mongol.*		Japan Sea*	
depth	velocity	depth	velocity	depth	velocity	depth	velocity
0.	3.43	0.	3.43	0.	2.87	0.	3.02
25.	3.52	22.	3.59	3.	3.74	4.	3.31
50.	4.30	45.	4.29	48.	4.54	16.	3.44
						26.	4.36

Tibet*		S. Mongol.*		N. China		S. China	
depth	velocity	depth	velocity	depth	velocity	depth	velocity
0.	2.74	0.	3.00	0.	3.21	0.	3.32
5.	3.38	3.	3.62	20.	3.72	18.	3.40
29.	3.37	43.	4.37	32.	4.33	33.	4.27
60.	4.23						